Received 29 April 2026; accepted 9 May 2026. Date of publication 13 May 2026;
date of current version 29 May 2026. The review of this article was coordinated by Editor M. Asad.

Digital Object Identifier 10.1109/OJVT.2026.3692885

A Novel Sensor Model-Based Object Existence Probability Fusion for Automotive Track-to-Track Fusion

JENŐ BÓKA [1], LÁSZLÓ LINDENMAIER [2], SZILÁRD ARADI [2,3] (Senior Member, IEEE), AND TAMÁS BÉCSI [2] (Senior Member, IEEE)

[1] VIE Technology Europe, 1117 Budapest, Hungary
[2] Department of Control for Transportation and Vehicle Systems, Faculty of Transportation Engineering and Vehicle Engineering, Budapest University of Technology and Economics, 1111 Budapest, Hungary
[3] Systems and Control Laboratory, HUN-REN Institute for Computer Science and Control (SZTAKI), 1111 Budapest, Hungary

CORRESPONDING AUTHOR: TAMÁS BÉCSI (e-mail: becsi.tamas@kjk.bme.hu).

This work was supported in part by the Ministry of Culture and Innovation, in part by the National Research, Development and Innovation Office within the Cooperative Technologies National Laboratory of Hungary under Grant 2022-2.1.1-NL-2022-00012, and in part by Project 2025-2.1.1-EKÖP through the Ministry of Culture and Innovation of Hungary from the National Research, Development and Innovation Fund, financed under Grant EKÖP-25-4-I funding scheme.

ABSTRACT Environment perception—and, in particular, multi-sensor fusion—plays a crucial role in ensuring the reliability of advanced driver assistance systems. Track-to-track fusion principles are widely adopted in automotive applications to combine object tracks generated by smart sensors. Within these systems, track management is a key component, as it strongly influences performance through track initiation and false-track suppression. State-of-the-art approaches address this problem by estimating and fusing the existence probabilities of tracks. Consequently, robust fusion of sensor-level existence estimates is essential for reliable track-to-track methods. In this paper, we extend our previous two-step hybrid existence probability fusion framework with probabilistic tracking and birth models. The proposed tracking model incorporates target velocity in addition to the sensor field of view, while the birth model captures the spatial context in which new objects are likely to emerge, enabling faster confirmation and improved false-track suppression. Experimental results obtained with a conventional radar–camera frontal perception setup demonstrate that integrating the proposed sensor models yields more than a 4% overall performance improvement, even within a standard one-step Dempster–Shafer belief fusion framework.

INDEX TERMS Advanced driver assistance systems, environment perception, multi-target tracking, probability fusion, sensor Modeling, smart sensors, track-to-track fusion.

I. INTRODUCTION

The Advanced Driver Assistant Systems (ADAS) play an important role in increasing the safety of road vehicles [1]. Efforts to reduce the frequency and severity of traffic accidents are strongly promoted by both the automotive industry and legislative bodies [2]. The reliability of these systems is crucial from both the user acceptance [3] and safety perspectives. Human drivers tend to over-rely on ADAS systems and fail to notice when they fail [4]. False alarms and actions (e.g., false emergency brake) usually stem from the malfunction of the environment perception system [5], [6]. Sensor fusion plays a vital role in improving the reliability of the perception system by combining information from multiple sensors and leveraging *a priori* knowledge of the different modalities [7], [8].

Sensor fusion can be realized at multiple abstraction levels, which highly impact the quality of the perception system. *Low-level* fusion, also referred to as *raw data fusion*, operates directly on sensor data throughout the entire processing pipeline, from raw measurements through feature extraction to detection, as in [9], [10]. As opposed to *low-level*, at *feature-level*, features are first extracted from the raw sensor data (separately from the fusion process), while tracking and fusion are performed centrally [11].

In *high-level* fusion, feature extraction and detection are performed by the sensors, and the fusion process operates on the resulting object-level data [12]; accordingly, this approach is also referred to as *object-level* fusion. Performing sensor fusion at higher abstraction levels yields two main advantages: first, sensor communication bandwidth is reduced; second, the higher abstraction level allows more modularity by isolating the fusion logic from sensor-specific details [13]. For these reasons, most ADAS systems rely on object-level fusion.

Moreover, automotive smart sensors typically perform a multi-object tracking (MOT) on object detections, providing tracked objects with unique identifiers. These sensor tracks, called *local* tracks, can be fused by two principal approaches. In a *measurement-to-track* fusion scheme, local tracks are treated as individual measurements and fused centrally using a recursive Bayesian filter (e.g., Kalman filter), as in [14], [15]. However, Kalman filtering assumes statistically independent measurements, whereas local tracks are correlated due to the common process noise arising from the underlying target dynamics [16], thereby violating this assumption. This limitation motivates the *track-to-track fusion* (T2TF) paradigm commonly adopted in decentralized perception architectures, in which each sensor maintains its own tracker.

Track-to-track fusion generates a global, fused track set while explicitly accounting for inter-track correlations, making it well-suited for fusing locally estimated tracks from automotive smart sensors. Track management is a critical component of track-to-track fusion, as it maintains the global track list by initiating and confirming new tracks corresponding to targets entering the surveillance area, and by coasting and removing global tracks in the absence of consistent sensor support. If a new track is confirmed too early, the probability of false alarms increases; conversely, overly conservative initiation may delay the detection of real targets or cause short-lived objects to be missed altogether. Therefore, track management plays a key role in the overall quality of the fusion process and, by extension, the entire perception system. In this paper, we focus on estimating the existence probability of global tracks, which provides a principled basis for track management decisions, such as when to confirm or delete object tracks.

A. RELATED WORK

Track management has a significant impact on false track suppression and, consequently, on the performance of the perception system [17]. Therefore, it remains a major focus of research in object tracking systems [18]. A common characteristic of the different approaches is the distinction between *tentative tracks*, which are internally maintained but not yet reported to the system output, and *confirmed tracks*, which are released only after a confirmation process verifies their existence [19]. The counter-pair of confirmation, the track deletion or removal, aims to remove outdated tracks that are no longer updated by sensor measurements [20].

The vast majority of existing track management methods rely on Bayesian statistical principles to estimate the probability of track existence, which will later serve as a metric for track management. The IPDA (Integrated Probabilistic Data Association) [21] is one of the first methods to integrate track existence estimation into the Bayesian PDA (Probabilistic Data Association) [22] single-object tracking framework. While [23] adapts the integrated existence probability formulation for the multi-object tracking variant of PDA, the JPDA (Joint Probabilistic Data Association). Similarly to IPDA and JIPDA, the PMHT (Probabilistic Multi-Hypothesis Tracking) [24] is also extended to include the probability of track existence in [17] and [25]. After quantifying the track existence, practically, the tracks with existence probability above a given threshold (i.e., confirmation threshold) are confirmed, while those below a deletion threshold are removed from the track list [26]. In [19], a two-step alert–confirm track confirmation strategy is proposed. First, tentative tracks are initialized with a more permissive existence threshold, and then selectively revisited with a stricter threshold.

Besides Bayesian methods, multiple non-Bayesian heuristic approaches have been proposed for track management in multi-object tracking [27]. A widely used strategy is the M-out-of-N logic, where a tentative track is promoted to confirmed status if at least M out of the last N measurements are associated with it [28]. Despite its popularity, this approach exhibits several limitations: the parameters M and N are typically fixed and non-adaptive, and the decision logic does not explicitly account for sensor characteristics such as field of view or detection probability. A more statistically grounded alternative for track confirmation and deletion is the sequential probability ratio test (SPRT), which has been integrated into the PMHT algorithm in [29]. In [27], a hybrid method is introduced by deriving a Bayesian SPRT, comparing it with the Bayesian IPDA and the M/N logic.

Both Bayesian probabilistic and heuristic methods are used in automotive applications, as in [30], [31]. However, they are primarily designed for centralized tracking architectures that operate directly on measurements (i.e., detection) rather than on tracked objects. Although they are sometimes used for T2TF in distributed sensor networks, as M/N logic is implemented in [32]. In such settings, false sensor tracks may already exhibit temporal consistency due to local sensor-level tracking algorithms, making them difficult to suppress [26]. To address this limitation, IPDA and JIPDA have been adapted to decentralized tracking architectures in [33], [34], where the existence probabilities of local sensor tracks are explicitly incorporated into the estimation of fused-track existence. Furthermore, the Dempster–Shafer method has been introduced for fusing the existence probabilities of track estimates in [35], [36]. Since Dempster–Shafer theory (DST) [37] generalizes Bayesian probability, it enables a more expressive representation of uncertainty. In our previous work [38], we proposed a hybrid two-step method combining *Dempster-Shafer* and cumulative belief fusion.

All these probabilistic approaches explicitly incorporate sensor characteristics and key parameters—such as detection, survival, and birth probabilities—that strongly influence tracking performance. In aerospace applications, where IPDA and JIPDA were originally introduced, these probabilities within the underlying Markov process were typically modeled as constants, reflecting the 360° field of view (FoV) of airborne and ground-based radar systems. In contrast, automotive applications must account for the limited FoV of onboard sensors, which necessitates more elaborate modeling. One of the simplest strategies is to use two constant detection probabilities—one inside and one outside the FoV—as in [39]. More refined approaches model detection probability as a function of the track's position relative to the sensor FoV [40], [41]. In [42], the detection probability is formulated as the product of three components: an FoV-dependent term analogous to the survival probability, the true positive detection probability, and a track-related term accounting for state uncertainty. Additionally, object occlusion is incorporated into the detection model in [30], [43]. The survival probability—also referred to as persistence probability—is frequently modeled as FoV-dependent, with reduced values near the boundaries of the surveillance region [30], [42], reflecting the assumption that targets cannot be maintained outside the observable area. Nevertheless, in many implementations, it is still represented by condition-dependent constants [40]. The birth probability is also often defined as a constant [42]. However, in [30], it is defined proportional to the gradient of the persistence probability, resulting in increased values in regions where persistence changes rapidly—such as at FoV boundaries or occlusion edges. A different assumption is made in [41], where new objects are prevented from being initiated in close proximity to existing tracks. Similarly, [40] derives the birth probability adaptively from an occupancy grid representation of the environment.

B. CONTRIBUTIONS OF THE PAPER

In contrast to the probability estimation methods integrated into traditional centralized tracking systems, the track-to-track existence probability fusion approaches proposed in [35], [36] adopt a more simplified parameterization. Among the probabilistic parameters discussed above, only the persistence probability is explicitly used, following [42]. Additionally, a sensor-dependent constant, referred to as the trust probability, is introduced to reflect the overall reliability of the sensors. However, detection and birth probabilities are not explicitly formulated at the fusion level. In this sense, the fusion process does not account for the spatial context in which tracks emerge, such as their proximity to FoV boundaries, even though such information may be relevant for assessing track existence.

Moreover, [35] and [36] rely exclusively on *Dempster-Shafer* (DS) theory for existence probability fusion. However, the application of Dempster's rule beyond the combination of belief constraints has been subject to criticism—particularly when independent belief estimates from multiple sources are fused cumulatively. Recognizing this limitation in the context of track existence fusion within a sensor-to-global architecture (i.e., T2TF with memory), we previously proposed a novel hybrid two-step framework [38]. The method combines Dempster's rule for sensor-to-sensor fusion with a cumulative fusion rule at the sensor-to-global level. For a detailed description, the reader is referred to [38].

In this paper, we extend that framework by introducing advanced probabilistic sensor-parameter models that more accurately capture and integrate sensor characteristics. The main contributions are summarized as follows:

- We propose a field-of-view-aware tracking model, analogous to persistence and detection probabilities, which additionally accounts for target velocity.
- We introduce a complementary birth model that incorporates the spatial context in which new objects are likely to appear.
- We reformulate the basic belief assignments presented in [38] to integrate these sensor-dependent characteristics into the two-step track-to-track existence probability fusion framework.

The proposed approach enables faster track confirmation and more effective false-track suppression, thereby improving the robustness and reliability of track-to-track fusion in automotive perception systems. The rest of the paper is organized as follows. The theoretical background of the topic is summarized in Section II. The final existence probability fusion method, extended with the proposed sensor model, is detailed in Section III. The experimental setup is described in Section IV, and the evaluation results are presented in Section V. Finally, the conclusions are drawn, with a brief outlook for future work, in Section VIII.

II. THEORETICAL BACKGROUND

This section presents the theoretical foundations for fusing the existence probabilities of tracks obtained from multiple independent sources. Consider a tracking system comprising two independent sensors, i and j, observing a target x^t. Let $x_k^{t_i}$ and $x_k^{t_j}$ denote the local tracks provided at the k-th time by sensors i and j, respectively, corresponding to the target x^t. The objective is to determine the existence probability $p(\exists x_k^{t_f})$ of the fused track $x_k^{t_f}$. Since most tracking algorithms incorporate an integrated estimation of track existence probability, as discussed in Section I-A, a clear approach is to combine the sensor-level existence probabilities $p(\exists x_k^{t_i})$ and $p(\exists x_k^{t_j})$ associated with $x_k^{t_i}$ and $x_k^{t_j}$.

The fusion of these probabilities can be performed according to two principal strategies: sensor-to-sensor and sensor-to-global, illustrated in Fig. 1(a) and Fig. 1(b), respectively. In the sensor-to-sensor strategy, asynchronous sensor tracks are buffered for several cycles and fused at the fixed sampling rate of the fusion module. This approach constitutes a purely feedforward architecture without feedback or persistent global memory. In contrast, the sensor-to-global strategy maintains global tracks over time and fuses incoming local sensor tracks with these stored global representations rather than directly with other local sensor tracks. For this reason, the sensor-to-global approach is commonly referred to as track-to-track

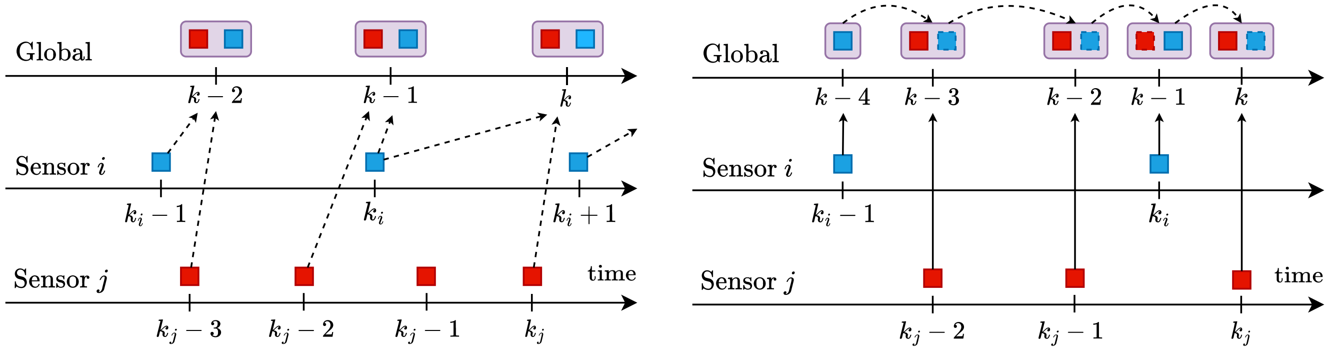

(a) Sensor-to-sensor strategy (b) Sensor-to-global strategy

FIGURE 1. Illustration of the different track-to-track fusion strategies with asynchronous sensor data. Dashed lines indicate that the corresponding track is predicted for the cycle they point to.

fusion with memory. Owing to the global representation, the sensor-to-global strategy offers structural advantages over the simpler sensor-to-sensor approach.

Dempster–Shafer theory, as a generalization of Bayesian probability, was first applied to existence probability fusion by Aeberhard et al. [35], employing belief fusion within a sensor-to-sensor framework. The method was subsequently extended to a sensor-to-global architecture in [36]. The following subsections introduce the fundamentals of Dempster–Shafer theory in the context of track existence probability fusion and present its derivation to both the sensor-to-sensor and sensor-to-global fusion strategies.

A. DEMPSTER-SHAFER THEORY

Dempster–Shafer belief fusion generalizes Bayesian probability by assigning belief masses to all subsets of the hypothesis space rather than restricting probability to single, mutually exclusive hypotheses. Let X denote the hypothesis space defined as $X = \{\exists, \nexists\}$, where $\exists$ and $\nexists$ represent the hypotheses corresponding to track existence and non-existence, respectively. The associated power set 2^X consists of all possible subsets of X:

$$2^X = \{\emptyset, \{\exists\}, \{\nexists\}, \{\exists, \nexists\}\}\,, \tag{1}$$

where $\exists, \nexists$ denotes the composite (uncertain) hypothesis. By explicitly allowing belief mass to be assigned to this set, Dempster–Shafer theory provides a more expressive representation of uncertainty than classical Bayesian probability. Then, a belief mass $m(\alpha)$ is assigned to each $\alpha \in 2^X$ such that the following conditions hold:

$$m(\alpha) \in [0, 1] \wedge m(\emptyset) = 0 \wedge \sum_{\alpha \in 2^X} m(\alpha) = 1\,. \tag{2}$$

This mapping is called the basic belief assignment (BBA). To combine information from multiple sources, the BBAs must be fused. Dempster's rule [37] defines an optimal operator to fuse belief constraints of different sources as follows:

$$m_k^{t_f}(\alpha) = (m_k^{t_i} \oplus m_k^{t_j})(\alpha) = \frac{\sum_{\beta\cap\gamma=\alpha} m_k^{t_i}(\beta) m_k^{t_j}(\gamma)}{1 - \sum_{\beta\cap\gamma=\emptyset} m_k^{t_i}(\beta) m_k^{t_j}(\gamma)}\,, \tag{3}$$

where $m_k^{t_i}$ and $m_k^{t_j}$ denote the BBAs at time k associated with the local tracks $x_k^{t_i}$ and $x_k^{t_j}$, respectively, and $m_k^{t_f}$ represents the resulting fused belief mass. Since the track management relies on the single-hypothesis Bayesian existence probability, it is computed from the fused belief masses as

$$p(\exists x_k^{t_f}) = m_k^{t_f}(\{\exists\}) + \frac{1}{2} m_k^{t_f}(\{\exists, \nexists\})\,, \tag{4}$$

The derivation of Dempster's rule for the existence probability fusion in the sensor-to-sensor and sensor-to-global strategies is presented in the following subsections, along with the corresponding BBAs.

B. BBA OF SENSOR-TO-SENSOR STRATEGY

Dempster's rule was first applied for existence probability fusion by Aeberhard et al. [35], exposing the BBA for a sensor-to-sensor strategy. According to [35], the mass beliefs of a local track, $x_k^{t_i}$, from sensor i are defined as

$$m_k^{t_i}(\{\exists\}) = p_{\text{trust}}^i \cdot p_{\text{pers}}^i(\hat{x}_k^{t_f}) \cdot p(\exists x_k^{t_i}) \tag{5}$$

$$m_k^{t_i}(\{\nexists\}) = p_{\text{trust}}^i \cdot p_{\text{pers}}^i(\hat{x}_k^{t_f}) \cdot (1 - p(\exists x_k^{t_i})) \tag{6}$$

$$m_k^{t_i}(\{\exists, \nexists\}) = 1 - (m_k^{t_i}(\{\exists\}) + m_k^{t_i}(\{\nexists\}))\,, \tag{7}$$

where p_{trust}^i denotes the trust probability of sensor i, and $p_{\text{pers}}^i(\hat{x})$ represents the persistence probability of the target as a function of its state, evaluated at the $\hat{x}_k^{t_f}$ fused state estimate. The underlying state fusion process is beyond the scope of this paper; further details can be found in [44]. The trust probability in [35] was defined as a sensor-dependent constant, and the persistence probability was given by the position of the tracks relative to the sensor FoV boundaries.

It may occur that no track from sensor i is assigned, through data association, to the track $x_k^{t_j}$ of sensor j. Such an unassignment may result from a misdetection at sensor i or from $x_k^{t_j}$ being a false track. This unassignment event is explicitly reflected in the corresponding BBA formulation:

$$m_k^{t_i}(\{\exists\}) = 0 \tag{8}$$

$$m_k^{t_i}(\{\nexists\}) = p_{\text{trust}}^i \cdot p_{\text{pers}}^i\left(\hat{x}_k^{t_f}\right) \tag{9}$$

$$m_k^{t_i}(\{\exists, \nexists\}) = 1 - p_{\text{trust}}^i \cdot p_{\text{pers}}^i\left(\hat{x}_k^{t_f}\right), \tag{10}$$

Note that, in case of two sensors, under unassignment $\hat{x}_k^{t_f} = \hat{x}_k^{t_j}$, as no corresponding track, nor state estimate is available from sensor i. Then, the BBA $m_k^{t_i}(\cdot)$ and $m_k^{t_j}(\cdot)$ of the track $x_k^{t_i}$ and $x_k^{t_j}$ from sensor i and sensor j, respectively, are fused into $m_k^{t_f}(\cdot)$, following the DS rule in (3).

C. BBA OF SENSOR-TO-GLOBAL STRATEGY

Subsequently, Dempster–Shafer theory was extended to the sensor-to-global strategy in [36], which maintains fused global tracks over time and predicts them from the $k-1$-th cycle to the k-th cycle, as illustrated in Fig. 1(b). In this framework, *a priori* belief masses are assigned not only to the local tracks but also to the predicted global track $x_{k|k-1}^{t_g}$:

$$m_{k|k-1}^{t_g}(\{\exists\}) = (1-\gamma) \cdot m_{k-1|k-1}^{t_g}(\{\exists\}) \tag{11}$$

$$m_{k|k-1}^{t_g}(\{\nexists\}) = (1-\gamma) \cdot m_{k-1|k-1}^{t_g}(\{\nexists\}) \tag{12}$$

$$m_{k|k-1}^{t_g}(\{\exists, \nexists\}) = 1 - (m_{k|k-1}^{t_g}(\{\exists\}) + m_{k|k-1}^{t_g}(\{\nexists\})), \tag{13}$$

where γ denotes the prediction weight, which increases the uncertainty during the prediction step. It may be chosen as a constant (typically $\gamma \approx 0$), but is more commonly modeled as a function of the time elapsed between the $(k-1)$-th and k-th cycles, such that longer prediction intervals yield larger values of γ.

After prediction, local sensor tracks are asynchronously associated with the predicted global tracks and fused accordingly. Specifically, when a local track $x_k^{t_i}$ is associated with the global track $x_{k|k-1}^{t_g}$, the *a priori* BBA defined in (11)–(13) is updated by combining it with the BBA of $x_k^{t_i}$ given in (5)–(7) using Dempster's rule in (3). If no local track from sensor i is associated with $x_{k|k-1}^{t_g}$, the predicted global track is instead fused with the BBA corresponding to the unassignment event defined in (8)–(10).

III. PROPOSED METHOD

In our previous work [38], we introduced a hybrid two-step existence probability fusion scheme, depicted in Fig 2, which combines the sensor-to-sensor and sensor-to-global strategies. The input to the fusion process is the so-called fused meta-track, $x_k^{t_f}$, obtained from the tracks belonging to the cluster $\mathcal{C}_k^{t_f}$. Note that in the example, depicted in Fig. 2, only two tracks of the two sensors comprise the cluster $\mathcal{C}_k^{t_f}$. For clarity, the example shown in Fig. 2 depicts a cluster comprising two tracks from two sensors; however, the proposed method is generic and not restricted to a two-sensor configuration. The data association and clustering procedures are beyond the scope of this paper; the reader is referred to [38] for details.

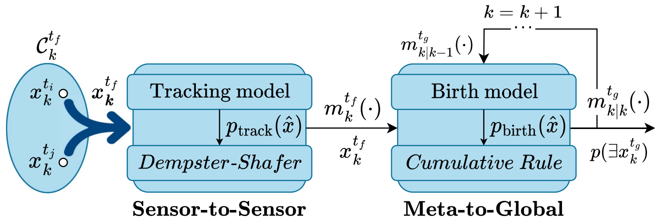

FIGURE 2. The illustration of the two-step track existence probability fusion in [38] extended with the proposed tracking and birth models.

In the first step, a conventional sensor-to-sensor fusion is performed using the *Dempster–Shafer* framework, as described in Sections II-A and II-B. This step determines the $m_k^{t_f}$ belief masses for the meta-track $x_k^{t_f}$. In the second step, the belief masses of the meta-track are combined with the *a priori* BBA $m_k^{t_g}$ of the predicted global track according to (11)–(13). However, considering the limitations of Dempster's rule when the fused sources do not constitute independent belief constraints [45], the cumulative fusion rule is employed instead. In [38], we demonstrated that the performance of the two-step hybrid approach exceeds that of the conventional one-step fusion using Dempster's rule.

However, the method in [38] relied on a simplified sensor model in which sensor-dependent BBA parameters were represented by uniform constant values. In the present work, the two-step hybrid framework is extended by incorporating probabilistic tracking and birth models to improve performance through faster track confirmation and enhanced false-track suppression. The tracking model characterizes target observability across sensors, explicitly accounting for geometric constraints in cases of missed detections. The birth model describes the spatial likelihood of new track initiation, i.e., the regions where targets may enter the surveillance area. The proposed tracking and birth models are detailed in Sections III-A and III-B, respectively.

A. TRACKING MODEL

The proposed tracking model characterizes the probability $p_{\text{track}}^i(\hat{x})$ that a track with state $\hat{x}$ can be observed and maintained by sensor i, analogous to the detection probability in centralized tracking systems. This formulation allows the fusion process to account for situations in which a sensor does not contribute to a meta-track during the sensor-to-sensor step due to its limited FoV. Consequently, the fused existence belief $m_k^{t_f}(\exists)$ is not degraded as a result of misdetection outside the observable region. Within the proposed framework, the persistence probability is reformulated as the tracking probability by replacing p_{pers} with the proposed p_{track} in the BBA expressions given in (5)–(7) and (8)–(10). The fusion step is then carried out according to Dempster's rule in (3).

The tracking probability $p^i_{\text{track}}(\hat{x})$ is modeled as a function of the target position $\mathbf{p}$ and velocity $\mathbf{v}$ relative to the FoV boundaries of sensor i. The target position $\mathbf{p} = [p_x, p_y]^\top$ and velocity $\mathbf{v} = [v_x, v_y]^\top$, expressed in longitudinal and lateral coordinates, are obtained directly from the state estimate $\hat{x}^{t_f}_k$ of the meta-tack, as the state space is defined as:

$$\hat{x} = \begin{bmatrix} p_x & v_x & p_y & v_y \end{bmatrix}^\top, \tag{14}$$

The sensor FoV, denoted by $\mathcal{F}_i$, is modeled as a set of annular sectors $\mathcal{F}_i = \{\nu_i^{(1)}, \nu_i^{(2)}, \ldots, \nu_i^{(n_i)}\}$, each defined by angular limits $[\theta_{\min}, \theta_{\max}]$ and range limits $[r_{\min}, r_{\max}]$. For notational simplicity, sensor and target indices are omitted in the following.

First, the proximity of a target to the boundaries of an arbitrary ν annular sector is calculated using the signed distance function, $d_{\text{sg}}(\mathbf{p}, \nu)$ defined as

$$d_{\text{sg}}(\mathbf{p}, \nu) = \begin{cases} -\min\{d_{\text{rad}}(\mathbf{p}, \nu), d_{\text{ang}}(\mathbf{p}, \nu)\} & \text{if } \mathbf{p} \in \nu \\ \min\{d_{\text{rad}}(\mathbf{p}, \nu), d_{\text{ang}}(\mathbf{p}, \nu)\} & \text{else} \end{cases}, \tag{15}$$

unifying the distance to the two types of boundaries: the d_{rad} radial distances to the range limits (circular edges) and the d_{ang} Euclidean distances from the angular edges. Let $r = \|\mathbf{p}\|$ and $\theta = \text{atan2}(p_y, p_x)$ denote the polar coordinates of the track. Then, the radial distance to the ν annular sector with $r_{\min}$ and $r_{\max}$ range boundaries is computed as

$$d_{\text{rad}}(\mathbf{p}, \nu) = \min\left(|r - r_{\min}|, |\, r - r_{\max}|\right), \tag{16}$$

The distance d_{ang} to the angular boundaries is defined similarly as

$$d_{\text{ang}}(\mathbf{p}, \nu) = \min\left(d_{\text{ang}}(\mathbf{p}, \theta_{\min}), d_{\text{ang}}(\mathbf{p}, \theta_{\max})\right), \tag{17}$$

where the $d_{\text{ang}}(\mathbf{p}, \theta)$ angular distance to a specific angular edge θ is computed as

$$d_{\text{ang}}(\mathbf{p}, \theta) = \begin{cases} -p_x \sin\theta + p_y \cos\theta & \text{if } r_{\min} \le r \le r_{\max} \\ \infty & \text{otherwise} \end{cases} \tag{18}$$

where the second case indicates that the distance r is outside the range interval $[r_{\min}, r_{\max}]$; in this case, setting $d_{\text{ang}}(\mathbf{p}, \theta)$ to ∞ ensures that $d_{\text{sg}}(\mathbf{p}, \nu) = d_{\text{rad}}(\mathbf{p}, \nu)$.

The proposed model accounts not only for the target's position relative to the FoV boundaries but also for its velocity. The underlying rationale is that targets that have already been within the FoV typically remain tracked for a short period, even after crossing the boundary and leaving it. In contrast, targets that are just entering the FoV require track initialization, during which reliable perception is less likely. To capture this asymmetric behavior, we introduce the FoV boundary-relative velocity v_{in}, defined as the component of the target velocity directed toward the interior of the FoV:

$$v_{\text{in}}(\nu) = \hat{\mathbf{n}}_\nu \cdot \mathbf{v}\,, \tag{19}$$

where $\hat{\mathbf{n}}_\nu$ denotes the normal vector of the FoV boundary determined from the gradient of the signed distance function $d_{\text{sg}}(\mathbf{p}, \nu)$ with respect to the target position $\mathbf{p}$ as

$$\hat{\mathbf{n}} = -\nabla d_{\text{sg}}(\mathbf{p}, \nu)\,. \tag{20}$$

This boundary-relative velocity, v_{in}, allows us to distinguish between targets entering and exiting the FoV. A positive value indicates motion toward the interior of the FoV (i.e., entering), whereas a negative value corresponds to motion away from it (i.e., exiting).

The tracking probability $p_{\text{track}}(\hat{x}, \nu)$ associated with a single annular FoV sector ν is defined separately for points inside and outside the sector. It is determined by the signed distance function d_{sg} in (15) and the direction of motion v_{in} according to (19), as follows:

$$p_{\text{track}}(\hat{x}, \nu) = \begin{cases} \text{inside the sector } (d_{\text{sg}} \le 0): \\ \begin{cases} P_\downarrow(|d_{\text{sg}}|) & \text{if } |d_{\text{sg}}| < \delta \wedge v_{\text{in}} > 0 \\ P_{\max} & \text{otherwise} \end{cases} \\ \text{outside the sector } (d_{\text{sg}} > 0): \\ \begin{cases} P_\uparrow(|d_{\text{sg}}|) & \text{if } |d_{\text{sg}}| < \delta \wedge v_{\text{in}} \le 0 \\ P_{\min} & \text{otherwise} \end{cases} \end{cases} \tag{21}$$

where $P_{\min}$ and $P_{\max}$ define the minimum and maximum probability values. While $P_\uparrow$ and $P_\downarrow$ denote the transition functions, inspired by [36], describing the change in the probability near the FoV boundaries as

$$P_\downarrow(d_{\text{sg}}) = P_{\min} + (P_{\max} - P_{\min}) \exp\left[\frac{-\ln(\alpha)(d_{\text{sg}} - \delta)}{d_{\text{sg}}}\right] \tag{22}$$

$$P_\uparrow(d_{\text{sg}}) = P_{\min} + (P_{\max} - P_{\min}) \exp\left[\frac{-\ln(\alpha)\, d_{\text{sg}}}{d_{\text{sg}} - \delta}\right], \tag{23}$$

where α and δ denote the slope parameter and the boundary threshold, respectively. The evolution of the tracking probability in the vicinity of the FoV boundaries for the two cases (i.e., entering and leaving the FoV) is illustrated in Fig. 3. As shown in Fig. 3(a), in the leaving scenario, the tracking probability decreases once the target crosses the FoV boundary. In contrast, for entering targets, the tracking probability increases only after the boundary has been crossed, as depicted in Fig. 3(b).

Finally, the overall tracking probability $p^i_{\text{track}}(\hat{x})$ of sensor i is defined as

$$p^i_{\text{track}}(\hat{x}) = \begin{cases} P_{\max}, & \text{if } \exists x^{t_i}_k : x^{t_i}_k \in \mathcal{C}, \\ \max\limits_{\nu \in \mathcal{F}_i} p_{\text{track}}(\hat{x}, \nu), & \text{otherwise.} \end{cases} \tag{24}$$

The first case applies when the cluster $\mathcal{C}^{t_f}_k$ of the meta-track $x^{t_f}_k$ contains a local track $x^{t_i}_k$ from sensor i. In this situation, the tracking probability is treated analogously to a detection event: since sensor i actively contributes a track to the meta-track, it is assumed to track the corresponding target with a constant $P_{\max}$ probability. In contrast, when no track from

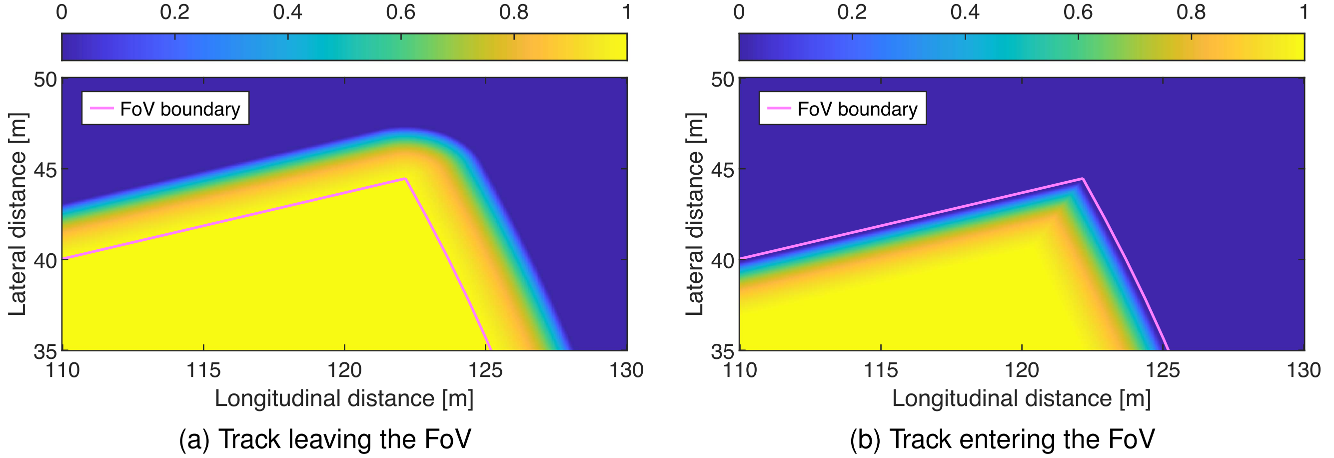

FIGURE 3. Illustration of the tracking probability transition depending on the velocity of the target.

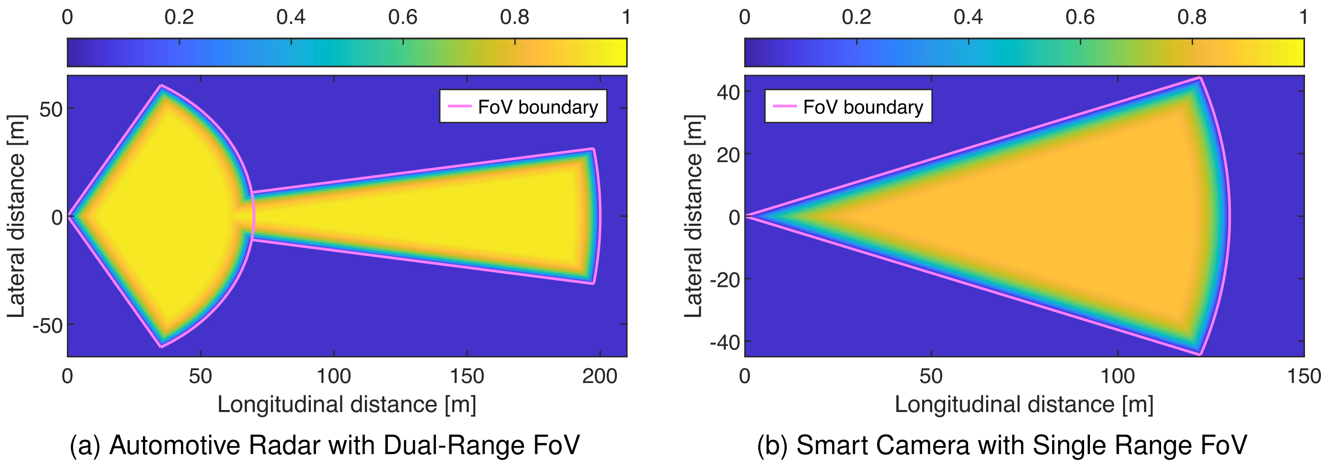

FIGURE 4. Illustration of the overall theoretical tracking probability of the sensors used in the experiments with $v_{\text{in}} \geq 0$.

sensor i is included in the meta-track $x_k^{t_f}$, the tracking probability reflects potential observability rather than an actual contribution. In this case, a theoretical tracking probability is computed as the supremum of the sector-wise probabilities $p_{\text{track}}(\hat{x}, \nu)$ over all annular sectors comprising the FoV. This geometric model quantifies the potential observability of the target by sensor i at state $\hat{x}$, even when no corresponding local track is available. The resulting overall theoretical tracking probability for the sensor configuration used in the experimental setup is illustrated in Fig. 4. As shown, the camera exhibits a lower peak tracking probability than the radar, which also features a dual-range FoV.

B. BIRTH MODEL

Using the revised tracking model alone may increase the occurrence of false tracks. Consider the case where sensor i generates a false local track $x_k^{t_i}$ in a region outside the FoV of sensor j. Owing to the low tracking probability $p^j_{\text{track}}(\hat{x})$, the fused belief $m_k^{t_f}(\exists)$ may remain high even though both $x_k^{t_i}$ and the resulting fused meta-track $x_k^{t_f}$ are false. To mitigate this effect, the proposed birth model characterizes the spatial likelihood of new track appearances via the probability $p_{\text{birth}}(\hat{x})$, highlighting where targets may enter the surveillance area.

Similarly to the tracking probability described earlier, the proposed birth probability $p_{\text{birth}}(\hat{x})$ is also formulated relying on the position $\mathbf{p}$ and the velocity $\mathbf{v}$ of the targets, again obtained from the state estimate $\hat{x}_k^{t_f}$ of the fused meta-track. First, the birth probability $p_{\text{birth}}(\hat{x}, \nu)$ for an arbitrary annular sector ν is calculated similarly to $p_{\text{track}}(\hat{x}, \nu)$ as

$$p_{\text{birth}}(\hat{x}, \nu) = \begin{cases} P_{\uparrow}(|d'_{\text{sg}}|) & \text{if } |d'_{\text{sg}}| < \delta \wedge v_{\text{in}} \geq 0 \\ P_{\min} & \text{otherwise} \end{cases}, \tag{25}$$

reusing the transition function $P_{\uparrow}$ defined in (22), along with the subsequent computations introduced in Section III-A. In contrast with $p_{\text{track}}(\hat{x}, \nu)$ in (21), (25) considers that new targets must move towards the FoV, i.e., those with $v_{\text{in}} \geq 0$; otherwise, $p_{\text{birth}}(\hat{x}, \nu)$ is set to a low value $P_{\min}$. To accommodate scenarios in which a newly appearing target is not immediately perceived and tracked by the sensor (e.g., distant targets), $P_{\min}$ should not be set to zero. This allows temporally

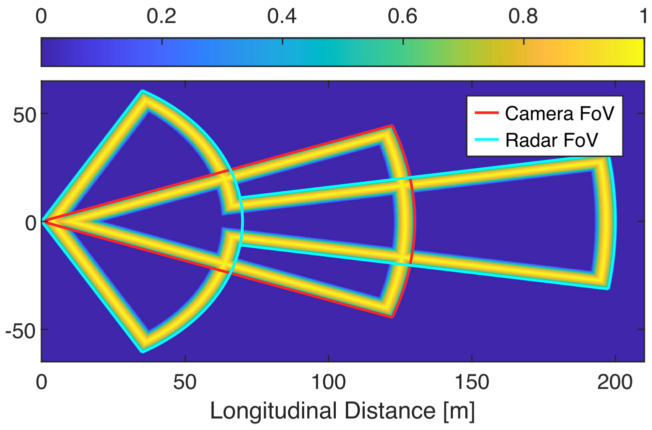

FIGURE 5. **Illustration of the overall birth probability map.**

consistent tracks with high existence probability to emerge beyond the FoV boundary. In (25), the modified signed distance d'_{sg} is defined as $d_{\text{sg}} + \Delta$, where Δ denotes an offset. The reason behind this offset is to ensure that the birth probability reaches a certain level $\mathcal{L} \cdot P$max already at the FoV boundary ($d_{\text{sg}} = 0$), supporting fast track confirmation in close proximity to the boundary. The offset is determined accordingly from the transition function $P_{\uparrow}$ as

$$\Delta = \frac{\ln(R) \cdot \delta}{\ln(\alpha) + \ln(R)}\,, \tag{26}$$

where R yields

$$R = \frac{\mathcal{L} \cdot P_{\max} - P_{\min}}{P_{\max} - P_{\min}}\,, \tag{27}$$

where $\mathcal{L}$ is set to 0.9 so that the birth probability already reaches 90% of $P_{\max}$ at the FoV boundary. Then, the birth probability $p^{i}_{\text{birth}}(\hat{x})$ with respect to sensor i is taken as the maximum of the sector-wise probabilities:

$$p^{i}_{\text{birth}}(\hat{x}) = \max_{\nu \in \mathcal{F}_i} p_{\text{birth}}(\hat{x}, \nu) \tag{28}$$

similar to (24). However, as seen in Fig. 2, in the second step of the fusion process, i.e, meta-to-global, the *a priori* belief masses $m^{t_g}_{k|k-1}(\cdot)$ are no longer fused with the sensors, but the BBA $m^{t_f}_{k}$ of the meta-track. Therefore, the overall birth probability $p_{\text{birth}}(\hat{x}^{t_f}_{k})$ is computed as the maximum over the set of sensors S:

$$p_{\text{birth}}\left(\hat{x}^{t_f}_{k}\right) = \max_{i \in S} p^{i}_{\text{birth}}\left(\hat{x}^{t_f}_{k}\right)\,, \tag{29}$$

The overall birth probability map of the experimental sensor set is depicted in Fig. 5.

The question arises how to incorporate the birth probability defined in (29) into the belief assignment. Directly reducing the belief mass $m^{t_f}_{k}(\exists)$ according to $p_{\text{birth}}(\hat{x}^{t_f}_{k})$ would indeed suppress false tracks in regions where spontaneous target appearance is unlikely. However, such a modification should affect only newly emerging tracks. To this end, track management distinguishes between tentative and confirmed global tracks. Each newly initialized global track is labeled as tentative. For meta-tracks assigned to a tentative global track $x^{t_g}_{k}$, the fused belief masses $m^{t_f}_{k}(\cdot)$ are adjusted as

$$\bar{m}^{t_f}_{k}(\{\exists\}) = p_{\text{birth}}(\hat{x}) \cdot m^{t_f}_{k}(\{\exists\}) \tag{30}$$

$$\bar{m}^{t_f}_{k}(\{\nexists\}) = m^{t_f}_{k}(\{\nexists\}) + (1 - p_{\text{birth}}(\hat{x})) \cdot m^{t_f}_{k}(\{\exists\}) \tag{31}$$

$$\bar{m}^{t_f}_{k}(\{\exists, \nexists\}) = 1 - (\bar{m}^{t_f}_{k}(\{\exists\}) + \bar{m}^{t_f}_{k}(\{\nexists\})) \tag{32}$$

before fusing with the *a priori* BBA $m^{t_g}_{k|k-1}$ of the according to the cumulative rule. A tentative global track $x^{t_g}_{k}$ is confirmed once its probability of existence $p(\exists x^{t_g}_{k})$ exceeds a predefined high threshold $p^{\exists}_{\text{thres}}$ (typically $p^{\exists}_{\text{thres}} \geq 0.9$). After confirmation, the birth model is no longer applied; specifically, it is replaced by $p_{\text{birth}}(\hat{x}) = 1$.

IV. EXPERIMENTAL SETUP

The experimental analysis is performed on a conventional forward-looking ADAS perception system, including an automotive Mobileye smart camera and a Continental ARS408-21 radar, both providing tracked objects. The ARS408-21 is a dual-mode radar (see Fig. 4(a)), featuring a near-range scan zone with a $\pm 60^{\circ}$ field of view (FoV) up to 70 meters, and a far-range scan zone extending up to 200 m with a narrower $\pm 9^{\circ}$ FoV. The Mobileye camera provides a $\pm 20^{\circ}$ FoV with a maximum detection range of 120 meters. The radar operates at 12 Hz, while the camera provides measurements at 9 Hz. Although the camera internally tracks a larger number of objects, due to communication bandwidth limitations, at most four tracks are transmitted. In contrast, the radar provides up to 50 tracks.

The evaluations are conducted in a high-fidelity simulation framework and using real-world measurements. First, two edge ADAS scenarios—an ACC (Adaptive Cruise Control) cut-in and an AEB (Autonomous Emergency Braking) full stop—are simulated using IPG CarMaker. The simulated trajectory represents a double-lane highway section bounded by guardrails, comprising a 900 m straight segment followed by a 90° circular arc with a radius of 750 m. Each scenario spans 40 seconds and involves six surrounding traffic participants, as illustrated in Fig. 6. In the ACC scenario, a peer vehicle cuts in between the ego vehicle and the target vehicle, forcing the ego vehicle to decelerate, while four additional vehicles contribute to a realistic traffic environment. The AEB scenario is more complex and dynamic, including an ego-vehicle lane change. Initially, the ego vehicle follows a leading vehicle, then performs a lane change to an adjacent lane behind two other vehicles. After approximately 400 m, these vehicles change lanes, revealing a stationary obstacle ahead. The ego vehicle decelerates and eventually stops behind the obstacle, while additional vehicles pass in the adjacent lane. The corresponding sensor data, i.e., tracked objects of the two smart sensors, are generated using the high-fidelity simulation framework in [46], which accounts for several sensor uncertainties, including missed and false detections and measurement noise.

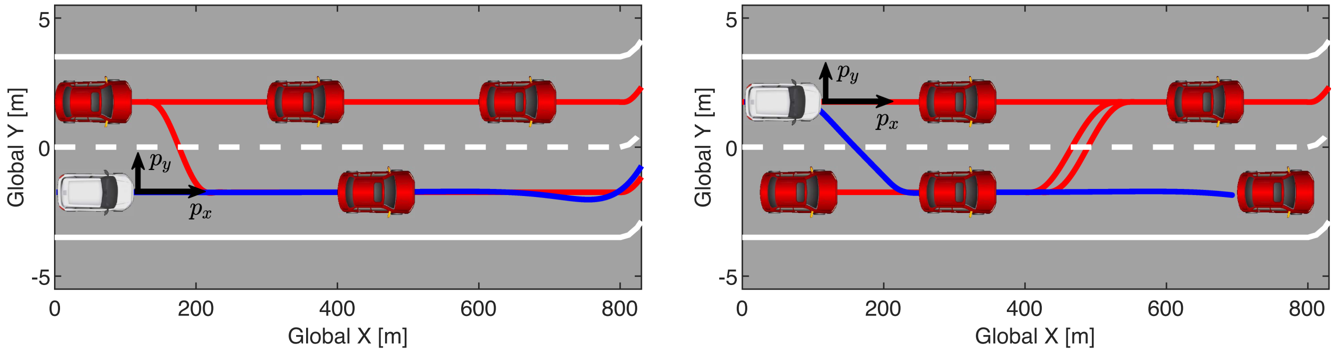

(a) Adaptive Cruise Control (ACC) cut-in (b) Autonomous Emergency Brake (AEB) full stop

FIGURE 6. The illustration of the simulated ADAS scenarios, where red and blue curves indicate the trajectory of the surrounding peer objects and the ego vehicle, respectively.

The real-world measurements are collected on the M1/M7 highway near Budapest under clear weather conditions during typical weekday afternoon traffic. As the raw image stream of the Mobileye camera is not accessible, the measurement platform was augmented with a synchronized monocular GoPro camera to support the evaluation alongside the radar and smart camera outputs. For the analysis, an approximately 8000-frame segment (about 130 seconds recorded at 60 FPS) was selected, intentionally covering dense traffic situations and dynamically challenging scenarios, including frequent lane changes and stationary vehicles in the emergency lane. The ground truth, i.e., the reference trajectories, was obtained through a semi-automatic annotation procedure based on [47]. The quantitative analysis is limited to a longitudinal distance of 90 m due to the increasing depth estimation uncertainty of the monocular camera, making reliable annotation challenging at long distances. In the lateral direction, the evaluation area is confined to ±20 m, since objects outside this corridor are typically disregarded by ADAS trajectory planning functions. Within this region, the ground-truth dataset contains 34,174 annotations corresponding to 26 distinct traffic participants, including passenger cars, trucks, and buses.

The evaluation is performed by computing the common object detection and multi-object tracking metrics, such as the precision, recall, F1 score, and MOTA. First, the resulting confirmed global tracks are associated with the reference objects of the ground truth, relying on the Kuhn-Munkres algorithm. The assignment is performed within cutoff distances of 10 and 1.5 meters in the longitudinal and lateral directions, respectively. An assignment between a fused track and a ground truth object is counted as a true positive, unassigned tracks are treated as false positives, and ground truth objects without corresponding tracks are considered false negatives. Precision and recall are then computed as

$$\text{Precision} = \frac{TP}{TP + FP}, \tag{33}$$

$$\text{Recall} = \frac{TP}{TP + FN}, \tag{34}$$

reflecting false detection suppression and detection completeness, where TP, FP, and FN denote the total number of true positives, false positives, and false negatives, respectively. The F1 score, defined as

$$F1 = \frac{2\,\text{Precision} \times \text{Recall}}{\text{Precision} + \text{Recall}}, \tag{35}$$

i.e., the harmonic mean of precision and recall provides an overall measure of detection performance. In addition, the MOTA metric evaluates conventional tracking quality, accounting for object identity consistency:

$$\text{MOTA} = 1 - \frac{FN + FP + IDS}{TP + FN}, \tag{36}$$

where IDS represents the number of identity switches across tracks.

V. PARAMETER IDENTIFICATION AND SENSITIVITY ANALYSIS

The parameters of the proposed tracking and birth models are systematically identified for both sensors. Since the four parameters—namely the minimum and maximum probabilities, $P_{\min}$ and $P_{\max}$, the boundary threshold δ, and the slope parameter α—are statistically correlated, making the joint identification of all parameters challenging. Therefore, $P_{\min}$ and $P_{\max}$ are fixed based on the following considerations. The minimum probability $P_{\min}$ for both the tracking and birth models is set to a small but nonzero value of 0.05. This choice ensures the gradual suppression of tracks outside the effective surveillance region, while still allowing confirmation of objects that do not strictly lie at the FoV boundary. For the birth model, the maximum probability $P_{\max}$ is set close to 1 for both sensors to enable rapid confirmation of newly appearing objects near the FoV limits. The maximum tracking probability $P_{\max}$ is explicitly determined by evaluating the tracking performance (i.e., recall) of the sensors. The radar can confidently detect and continuously track most targets, resulting in a relatively high probability value of 0.95. In contrast, the camera's peak tracking probability is limited to 0.85, reflecting its practical constraint of transmitting at

TABLE 1. Results of the Parameter Sensitivity (p-Value) Analysis

	Tracking Model		Birth Model	
Sensor	δ	α	δ	α
Camera	$\mathbf{4.54 \cdot 10^{-14}}$	$\mathbf{6.05 \cdot 10^{-4}}$	0.7457	$\mathbf{1.31 \cdot 10^{-4}}$
Radar	0.3764	0.5890	$\mathbf{6.88 \cdot 10^{-5}}$	$\mathbf{6.54 \cdot 10^{-22}}$

The bold values indicate the parameters with a significant ($p<0.05$) impact

TABLE 2. Parameters of the Proposed Models

	Tracking Model				Birth Model			
Sensor	$P_{\min}$	$P_{\max}$	δ	α	$P_{\min}$	$P_{\max}$	δ	α
Camera	0.05	0.85	**3.59**	**0.91**	0.05	0.98	**5.69**	**0.83**
Radar	0.05	0.95	**3.95**	**0.77**	0.05	0.98	**3.42**	**0.99**

most 4 tracks. The boundary threshold δ and slope parameter α are then identified via Monte Carlo simulation using the simulation framework described in Section IV. Specifically, for both ADAS scenarios illustrated in Fig. 6, tracked objects from the smart camera and radar are simulated using the end-to-end framework in [46]. A total of 120 parameter sets were generated within the ranges of $\delta \in [1, 7]$ and $\alpha \in [0.6, 1]$ using Latin Hypercube Sampling (LHS), ensuring a space-filling coverage of the parameter domain. The fusion output of each simulation is evaluated using the metrics described in Section IV, namely recall, precision, F1 score, and MOTA. To obtain a more representative dataset, results from the ACC cut-in and AEB scenarios are combined. Finally, the optimal parameter values are selected by maximizing the F1 score, which serves as the overall performance metric for the fusion.

Based on the results of the Monte Carlo simulation, a parameter sensitivity analysis is conducted by fitting a linear regression model to the identified parameters δ and α. The detailed outcomes of this regression are presented in the Appendix. The present discussion is restricted to parameter sensitivity, as quantified by the p-values reported in Table 1. The radar tracking model parameters have a limited impact on fusion performance compared to those of the camera. In contrast, for the birth model, the radar parameters exhibit a more pronounced influence than the camera parameters. This behavior can be explained by the sensor fields of view (FoVs) shown in Fig. 5. Targets passing the ego vehicle appear in the radar's wide-angle, near-range scan zone. Consequently, the parameter identification favors rapid track confirmation, resulting in a high slope value, while the boundary parameter is chosen to be sufficiently large to allow track confirmation, yet low enough to suppress false tracks. Conversely, the model must account for regions not covered by the camera, i.e., where radar-only tracks may occur; therefore, the camera's tracking model parameters have a more significant impact on overall fusion performance. Overall, the optimal parameter set achieves an F1 score of 96.85%, whereas the least effective configuration attains 91.73%, indicating that high performance is maintained even under suboptimal parameter choices. The resulting parameter set for the proposed models is summarized in Table 2, where bold entries indicate the identified parameters.

The trust probability p_{trust} of the sensors are adopted from our previous work in [38], as it is not part of the present models. These values were tuned empirically based on the following considerations. For the camera, p_{trust} is set to 0.99, reflecting that it provides at most 4 tracks with a very low false-detection rate. For the radar, it is set to 0.85 to account for its higher susceptibility to false detections from environmental structures, such as guardrails and highway overpasses.

VI. RESULTS

The proposed existence probability fusion method, comprising the probabilistic tracking and birth models, is evaluated through the following experiments:

- evaluation in two simulated ADAS edge scenarios, as discussed in Section VI-A;
- evaluation using real-world measurements collected on a highway section, as presented in Section VI-B;
- an ablation study to assess the individual contributions of the proposed tracking and birth models, as described in Section VI-C.

The performance of the proposed sensor model is compared with two reference approaches:

- the *uniform* model from our previous work [38], which assumes a constant tracking probability across the entire surveillance area; and
- the *FoV-aware* persistence probability model [35], [42], which reduces the persistence probability near the boundaries of the FoV.

As discussed earlier, the proposed sensor models are integrated into the two-step existence probability fusion framework introduced in our previous work [38]. Their impact is evaluated using the performance metrics defined in Section IV, and compared against the aforementioned baseline approaches, each substituted into the same two-step fusion structure in place of the proposed model. To further assess the influence of the sensor modeling, the same comparison is conducted within the one-step existence probability fusion scheme based on Dempster's rule, as presented in [36].

A. SIMULATION RESULTS

First, the evaluation is performed on the two edge ADAS scenarios illustrated in Fig. 6 simulating the sensor data using [46], as described in Section IV. It should be mentioned that the parameter identification is performed on the same scenarios, but the sensor disturbances differ between runs due to their stochastic realization. The resulting performance metrics evaluations on the ACC and AEB scenarios are summarized in Tables 3 and 4, respectively.

In the ACC scenario, the proposed model within the two-step fusion framework achieves a substantial improvement

TABLE 3. Evaluation Results of the Simulated ACC Scenario (Fig. 6(a))

Fusion	Model	Precision [%]	Recall [%]	F1 [%]	MOTA [%]
Two-step [38]	Uniform [38]	**98.96**	81.14	89.17	80.27
	FoV-aware [42]	82.59	**95.73**	88.68	75.53
	Proposed	97.12	94.75	**95.92**	**91.92**
One-step [36]	Uniform [38]	**98.33**	80.64	**88.61**	**79.23**
	FoV-aware [42]	57.86	86.31	69.28	23.40
	Proposed	85.78	**87.57**	86.67	73.03

TABLE 4. Evaluation Results of the Simulated AEB Scenario (Fig. 6(b))

Fusion	Model	Precision [%]	Recall [%]	F1 [%]	MOTA [%]
Two-step [38]	Uniform [38]	**97.94**	85.03	91.03	83.19
	FoV-aware [42]	86.98	**94.36**	90.52	80.21
	Proposed	96.84	94.13	**95.46**	**91.04**
One-step [36]	Uniform [38]	**96.15**	84.07	89.70	80.66
	FoV-aware [42]	64.15	87.82	74.18	38.74
	Proposed	93.54	**89.56**	**91.51**	**83.34**

over both baseline approaches. Compared to the FoV-aware persistence model, the proposed method increases precision by more than 14%, while maintaining a high recall close to the FoV-aware approach. This indicates that the proposed birth model effectively suppresses false tracks without significantly compromising tracking capability. In comparison to the uniform model, the proposed approach improves recall by more than 13% thanks to the tracking model accounting for the limited camera FoV in the near-range zone, while only slightly reducing precision. As a result, the proposed model achieves the highest overall performance, exceeding the baseline methods by 6.75% and 7.24% in F1 score, and by 11.65% and 16.39% in MOTA, respectively.

A similar trend can be observed in the one-step fusion framework. While the uniform model yields the highest precision (98.33%), it suffers from limited recall. In contrast, the proposed method improves recall by nearly 7% compared to the uniform model. However, its precision falls short of the uniform model due to a false track appearing near the radar's FoV boundary; thus, it is confirmed by the birth model. Compared to the FoV-aware model, the proposed approach achieves a significant precision gain of nearly 28%, highlighting its robustness against false tracks generated by guardrails thanks to the birth model. Consequently, the proposed model improves the F1 score by 18.06% and 1.06%, and the MOTA metric by 49.63% and 6.20% relative to the FoV-aware and uniform models, respectively, demonstrating a clear advantage in overall tracking performance.

In the AEB scenario, the superiority of the proposed model becomes even more pronounced. Within the two-step fusion framework, the proposed approach achieves a balanced and high performance across all metrics, improving precision by approximately 10% over the FoV-aware model while maintaining a comparable recall. Compared to the uniform model, it significantly increases recall by more than 9% with only a marginal decrease in precision. This leads to the highest F1 and MOTA scores, outperforming the baseline approaches by up to 4.94% and 10.83%, respectively.

The same tendency is reflected in the one-step fusion results for the AEB scenario. The proposed model consistently achieves the best trade-off between precision and recall, improving precision by more than 11% compared to the FoV-aware model and by 2.39% compared to the uniform approach. Furthermore, it provides the highest recall among the evaluated methods. As a result, the proposed method surpasses the baseline models by 17.33% and 1.81% in F1 score, and by 44.60% and 2.68% in MOTA, respectively.

Overall, the simulated results confirm that the proposed model consistently provides a more favorable balance between false track suppression and track confirmation capability across different scenarios and fusion architectures. This leads to significant improvements in tracking performance, particularly in challenging conditions where the limitations of the field of view play a crucial role.

TABLE 5. Evaluation Results of Real-World Measurement

Fusion	Model	Precision [%]	Recall [%]	F1 [%]	MOTA [%]
Two-step [38]	Uniform [38]	97.66	79.55	87.68	77.63
	FoV-aware [42]	90.97	**87.94**	89.43	79.21
	Proposed	**97.97**	87.86	**92.64**	**86.03**
One-step [36]	Uniform [38]	95.10	73.34	82.78	69.46
	FoV-aware [42]	82.29	77.83	80.00	61.05
	Proposed	**96.54**	**79.41**	**87.14**	**76.55**

B. REAL-WORLD MEASUREMENT RESULTS

Besides the simulation scenarios, the evaluation is also performed using real-world measurements, as discussed in Section IV. The performance metrics of this evaluation is summarized in Table 5. According to these evaluation metrics, the proposed model achieves a 7% improvement in precision over the FoV-aware persistence model, indicating superior false-track suppression. This improvement stems from the ability of the proposed birth model to attenuate the existence probability of tracks appearing in regions distant from the FoV boundaries. As illustrated in Fig. 7(a), relying solely on the FoV-aware persistence model, as in [42], allows false tracks generated by the guardrail on the left to be confirmed, since this area is not covered by the camera. Although the uniform model already attains a high precision of 97.66%, the proposed approach further increases it by 0.31%. In terms of recall, the proposed method surpasses the uniform model

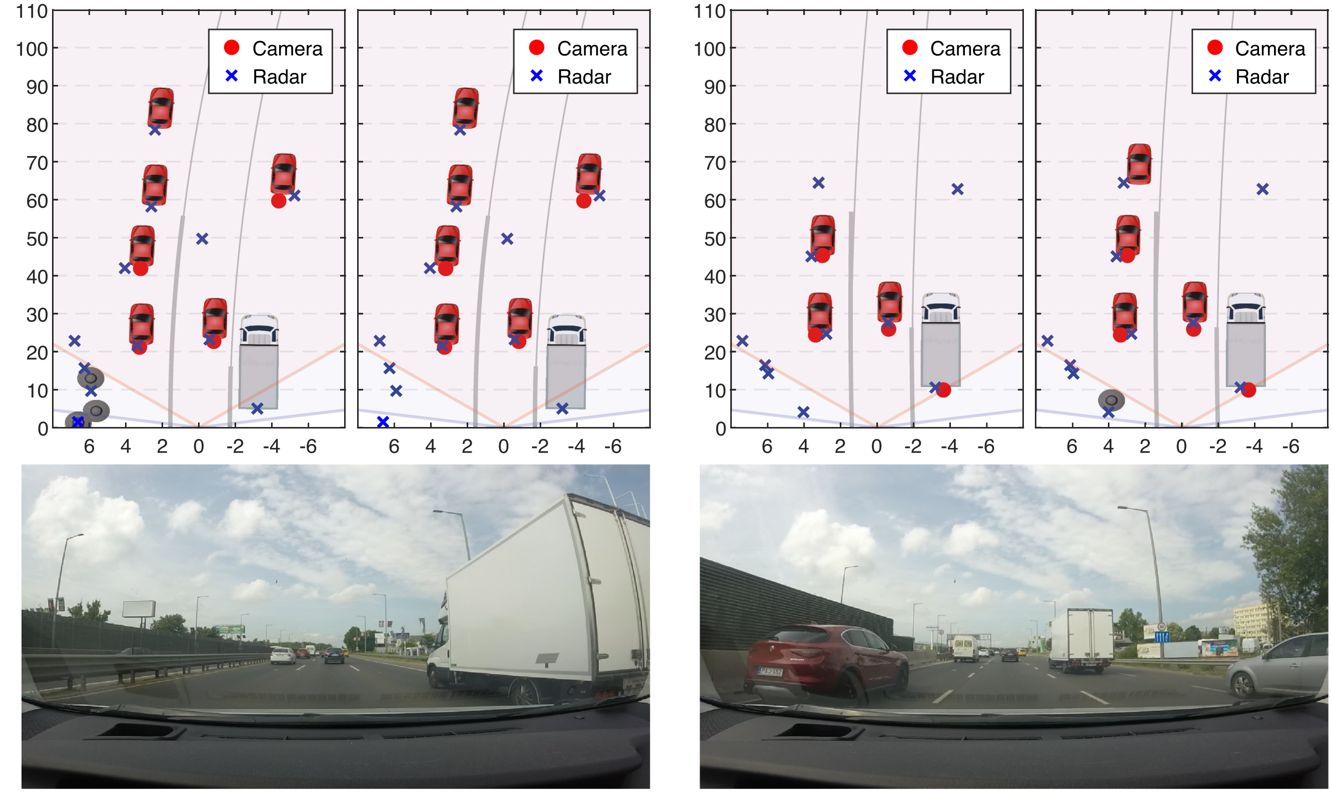

(a) FoV-aware persistence probability in [42] (left) compared to the proposed model (right)

(b) Uniform sensor model employed in [38] (left) compared to the proposed one (right)

FIGURE 7. **Qualitative comparison of the evaluated sensor models illustrated by the confirmed tracks represented with the icons in the bird's-eye-view plane (UFO symbols indicate unknown object classifications, since the radar does not provide class information).**

by more than 8%, owing to the tracking probability formulation that explicitly accounts for the limited FoV angle of the camera relative to the radar. This enables confirmation of tracks within the wider near-range scan zone of the radar, as highlighted in Fig. 7(b) by the UFO icon on the left. While the recall of the proposed method is slightly lower than that of the FoV-aware persistence model, it still outperforms both baseline methods in the overall detection and tracking indicators, achieving gains of 4.96% and 3.21% in F1 score, and 8.40% and 6.82% in MOTA, respectively.

A similar tendency is observed within the one-step fusion framework of [36]. In this case, the proposed model further enhances false track suppression compared to the uniform and FoV-aware approaches, yielding precision gains of 1.93% and 14.74%, respectively. Moreover, it achieves the highest recall (79.24%), demonstrating improved track confirmation capability. Consequently, the proposed model exceeds the baseline methods by 4.46% and 7.24% in F1 score, and by 7.35% and 15.76% in MOTA, respectively.

Although some differences can be observed between the simulation and real-world evaluation results, the results obtained from real-world measurements confirm the same tendency as in the simulation studies. In particular, the proposed model improves overall detection and tracking performance compared to the baseline approaches, while maintaining stable precision levels despite the increased complexity and noise of real driving data. These findings demonstrate that the advantages of the proposed models generalize beyond simulated environments and remain effective under realistic measurement conditions. The slightly lower recall observed in the real-world experiments can be attributed to the higher complexity of the highway scenario, which involves dense traffic conditions compared to the limited number of six targets considered in the simulation setup.

C. ABLATION STUDY

Finally, an ablation study is conducted on the real-word measurements to analyze the individual contributions of the proposed tracking and birth models. To this end, the proposed method is evaluated by separately ablating each component: removing the birth model substitutes $p_{\text{birth}} = 1$ into (30)–(31), while removing the tracking model replaces p_{track} with a uniform $P_{\max}$ according to Table 2, as in [38]. The study is limited to the two-step fusion framework shown in Fig. 2, and the results are summarized in Table 6.

When the birth model is removed, a noticeable decrease in precision is observed (-5.70%), while recall remains largely unaffected (+0.14%). This indicates that the birth model primarily contributes to suppressing false tracks, considering that

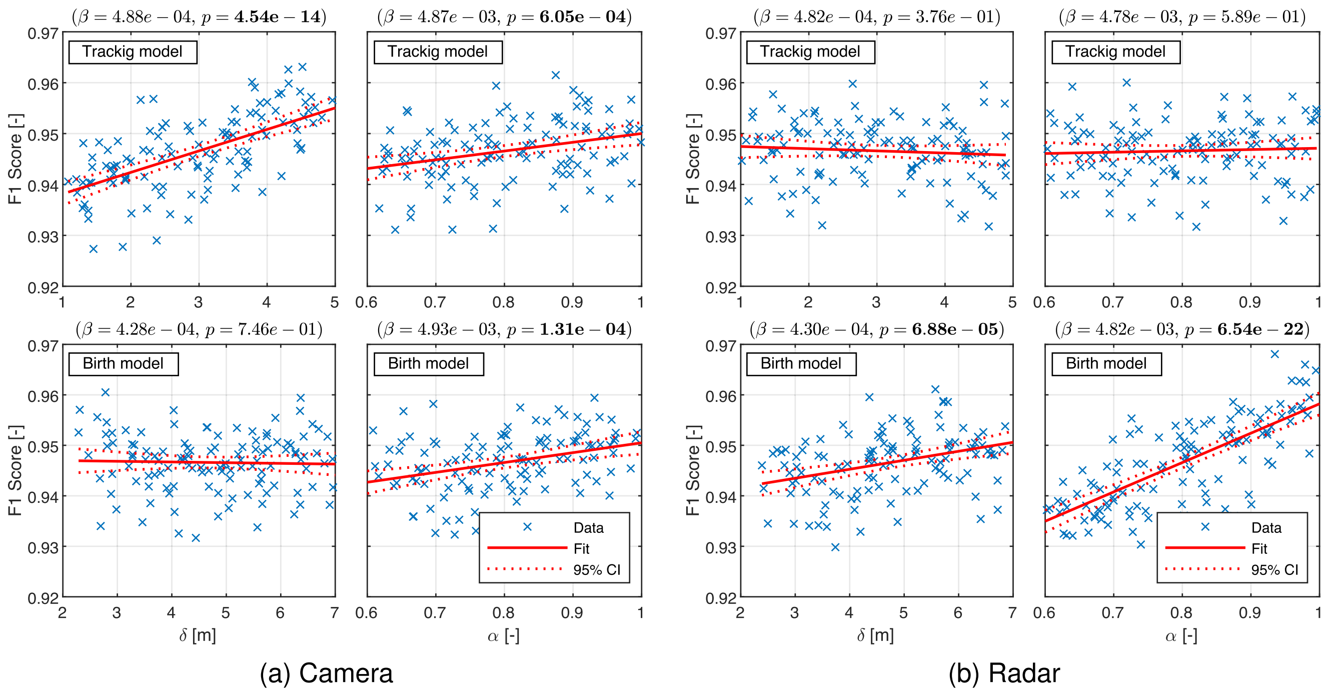

FIGURE 8. **Partial regression leverage plot of the identified model parameters, where β denotes the steepness of the fitted linear equations and p indicates the p-value of the parameters, while 95% CI stands for the 95% confidence interval.**

TABLE 6. **Results of Ablation Study**

Setup	Precision [%]	Recall [%]	F1 [%]	MOTA [%]
w/o Birth Model	92.27 (-5.70)	87.90 (+0.14)	90.03 (-2.61)	80.53 (-5.50)
w/o Tracking Model	97.70 (-0.27)	79.64 (-8.22)	89.43 (-4.89)	79.21 (-8.27)

The values in parentheses denote the change compared to the metrics of the proposed model in the two-step fusion framework in Table 5.

new targets may emerge at the edges of the FoVs. Its absence leads to an increased number of false positives, which also results in a degradation of the F1 score (-2.61%) and MOTA (-5.50%). In contrast, removing the tracking model has more impact on recall, which drops by 8.22%, while precision remains almost unchanged (-0.27%). This highlights that the tracking model plays a crucial role in maintaining track continuity and preventing premature track termination, thereby improving recall by explicitly modeling regions covered by a single sensor.

Overall, the ablation study demonstrates that the birth and tracking models contribute in complementary ways: the birth model enhances precision by mitigating false track initiations, while the tracking model improves recall by supporting sustained track existence. Their combined effect is essential for achieving the overall performance gains of the proposed fusion method.

VII. DISCUSSION AND LIMITATIONS

The experimental results demonstrate that the proposed sensor model, comprising the tracking and birth components, outperforms both baseline methods: the FoV-aware persistence model in [42] and the uniform model used in our previous work [38]. A key limitation of these approaches is the absence of a birth model, effectively assuming $p_{\text{birth}} = 1$. As a result, the FoV-aware model cannot adequately suppress false tracks, since it does not account for the spatial likelihood of track initiation. In particular, radar tracks in the near-range region outside the camera FoV—including false detections caused by guardrails—are incorrectly confirmed, leading to reduced precision. This effect is more pronounced in simulation, where guardrails are present along the entire scene, compared to the real-world dataset, where they appear only in limited sections. Another distinction is that the proposed tracking model employs a unified boundary-relative distance formula, rather than separate transition functions for angular and radial FoV limits, and additionally incorporates target velocity. Consequently, even without the birth model, it achieves higher precision (92.27%) than the FoV-aware persistence model (90.97%).

Compared to the uniform model, the proposed method significantly improves detection and tracking performance, increasing recall by more than 8% while maintaining almost the same high precision. This gain stems from the complementary roles of the tracking and birth models, as confirmed by the ablation results in Table 6: the tracking model supports the confirmation of radar-only tracks in regions not covered by the camera, while the birth model suppresses false tracks by reducing their probability outside plausible entry regions.

A limitation of the proposed method is illustrated by the simulated ACC scenario, where a false track appears near the radar FoV boundary, mimicking the entry of a new target. As shown in Table 3, this leads to a precision drop of more than 12% in the one-step fusion framework compared to the uniform model. However, in the two-step fusion framework, this false track is effectively filtered out due to the smoother temporal evolution of the existence probability. This further confirms that the two-step fusion approach proposed in [38] improves not only track continuity (recall) but also robustness against false track confirmations.

Another limitation of this work is that the experiments are restricted to structured environments, such as highways. Future work will therefore focus on validation in unstructured urban scenarios. Nevertheless, high-level track-to-track fusion methods are typically designed for structured environments. Although the experiments consider a conventional forward-looking ADAS sensor setup comprising a radar and a camera, the proposed method is generic and can be extended to an arbitrary number of smart sensors providing tracked objects with associated existence probabilities.

VIII. CONCLUSION

In this paper, we introduced novel sensor models that extend our previous track-to-track existence probability fusion framework. The proposed approach comprises a probabilistic tracking and a birth model. The tracking probability is derived from the signed distance to the sensor field-of-view boundary and additionally incorporates the target velocity, enabling more informed handling of objects near FoV limits. This formulation facilitates track confirmation in regions covered by only a subset of the sensors. In addition, a birth probability model is proposed to characterize areas where new objects are likely to appear, enabling effective suppression of false tracks in areas where spontaneous object appearance is unlikely. Experimental results demonstrate that the fusion framework augmented with the proposed sensor models significantly outperforms both our earlier uniform sensor model and an existing FoV-aware approach across object detection and tracking performance metrics.

Future research will focus on incorporating the proposed models into centralized multi-object tracking frameworks, such as GM-PHD filters. Moreover, the development of an adaptive clutter (false detection) model is planned. Finally, deep learning techniques will be investigated to further enhance model adaptability and performance.

APPENDIX

The detailed results of the linear regression models fitted to the boundary threshold δ and slope parameter α are shown in Figs. 8(a) and (b) for the camera and radar, respectively. The partial regression leverage plots in Fig. 8, also known as added-variable plots, illustrate the incremental effect of each parameter on overall performance (i.e., F1 score) after removing the influence of the remaining parameters. However, these plots should not be interpreted to imply that a positive regression coefficient (β) indicates that the highest parameter values are preferable. Rather, they show statistical correlation and extend the insights provided in Table 1.

REFERENCES

[1] A. J. Benson, B. C. Tefft, A. M. Svancara, and W. J. Horrey, "Potential reductions in crashes, injuries, and deaths from large-scale deployment of advanced driver assistance systems," *Res. Brief*, 2018. [Online]. Available: https://aaafoundation.org/wp-content/uploads/2026/01/18-0567_AAAFTS-ADASPotential-Benefits-Brief_v2.pdf

[2] European Commission, "EU road safety policy framework 2021-2030 Next steps towards 'Vision Zero'," 2020. [Online]. Available: https://op.europa.eu/en/publication-detail/-/publication/d7ee4b58-4bc5-11ea-8aa5-01aa75ed71a1

[3] M. W. Khattak, K. Brijs, T. M. Tran, T. A. Trinh, A. T. Vu, and T. Brijs, "Acceptance towards advanced driver assistance systems (ADAS): A validation of the unified model of driver acceptance (UMDA) using structural equation modelling," *Transp. Res. Part F, Traffic Psychol. Behav.*, vol. 105, pp. 284–305, 2024.

[4] V. Ötvös, S. Szigeti, É. Barna, and Á. Török, "Advanced driver assistance systems in the driver training system in Hungary," *Periodica Polytechnica Transp. Eng.*, vol. 54, no. 1, pp. 80–87, 2026.

[5] S. Jiang and J. Zhang, "Association analysis of ADAS and ADS accidents: A comparative study based on association rule mining," *Appl. Sci.*, vol. 15, 2025, Art. no. 13146.

[6] L. Zhang, Z. Yu, X. Xu, and Y. Yan, "Research on automatic emergency braking system based on target recognition and fusion control strategy in curved road," *Electron.*, vol. 12, no. 16, 2023, Art. no. 3490. [Online]. Available: https://www.mdpi.com/2079-9292/12/16/3490

[7] H. Zhu, K.-V. Yuen, L. Mihaylova, and H. Leung, "Overview of environment perception for intelligent vehicles," *IEEE Trans. Intell. Transp. Syst.*, vol. 18, no. 10, pp. 2584–2601, Oct. 2017.

[8] J. Vargas, S. Alsweiss, O. Toker, R. Razdan, and J. Santos, "An overview of autonomous vehicles sensors and their vulnerability to weather conditions," *Sensors*, vol. 21, no. 16, 2021, Art. no. 5397.

[9] P. Wolters et al., "Unleashing HyDRa: Hybrid fusion, depth consistency and radar for unified 3D perception," *Proc. IEEE Int. Conf. Robot. Automat.*, Atlanta, GA, USA, 2025, pp. 7467–7474.

[10] Z. Lin, Z. Liu, Y. Wang, L. Zhang, and C. Zhu, "RCBEVDet++: Toward high-accuracy radar-camera fusion 3D perception network," 2024, *arXiv:2409.04979*.

[11] N. Kaempchen, M. Buehler, and K. Dietmayer, "Feature-level fusion for free-form object tracking using laserscanner and video," in *Proc. IEEE Proc. Intell. Veh. Symp.*, 2005, pp. 453–458.

[12] T. Osterburg, F. Albers, C. Diehl, R. Pushparaj, and T. Bertram, "HiLO: High-level object fusion for autonomous driving using transformers," *IEEE Intell. Veh. Symp.*, Cluj-Napoca, Romania, 2025, pp. 209–214.

[13] M. Aeberhard and N. Kaempchen, "High-level sensor data fusion architecture for vehicle surround environment perception," in *Proc. 8th Int. Workshop Intell. Transp.*, 2011, vol. 665, pp. 1–7.

[14] F. Fayad and V. Cherfaoui, "Object-level fusion and confidence management in a multi-sensor pedestrian tracking system," in *Proc. IEEE Int. Conf. Multisensor Fusion Integration Intell. Syst.*, 2008, pp. 58–63.

[15] H. Cho, Y.-W. Seo, B. V. Kumar, and R. R. Rajkumar, "A multi-sensor fusion system for moving object detection and tracking in urban driving environments," in *Proc. IEEE Int. Conf. Robot. Automat.*, 2014, pp. 1836–1843.

[16] Y. Bar-Shalom, "On the track-to-track correlation problem," *IEEE Trans. Autom. Control*, vol. AC-26, no. 2, pp. 571–572, Apr. 1981.

[17] D. Musicki and X. Wang, "Track management and PMHT," in *Proc. 10th Int. Conf. Inf. Fusion*, 2007, pp. 1–5.

[18] D. Stadler and J. Beyerer, "Improving multiple pedestrian tracking by track management and occlusion handling," in *Proc. IEEE/CVF Conf. Comput. Vis. Pattern Recognit.*, 2021, pp. 10958–10967.

[19] I. V. L. Clarkson and J. L. Williams, "An alert-confirm approach to track confirmation," in *Proc. 52nd Asilomar Conf. Signals, Syst., Comput.*, 2018, pp. 1169–1173.

[20] M. Dimitrievski, D. Van Hamme, P. Veelaert, and W. Philips, "Cooperative multi-sensor tracking of vulnerable road users in the presence of missing detections," *Sensors*, vol. 20, no. 17, 2020, Art. no. 4817.

[21] D. Musicki, R. Evans, and S. Stankovic, "Integrated probabilistic data association," *IEEE Trans. Autom. Control*, vol. 39, no. 6, pp. 1237–1241, Jun. 1994.

[22] Y. Bar-Shalom and X.-R. Li, *Multitarget-Multisensor Tracking: Principles and Techniques*. Storrs, CT, USA: YBS Publishing, 1995.

[23] D. Musicki and R. Evans, "Joint integrated probabilistic data association: JIPDA," *IEEE Trans. Aerosp. Electron. Syst.*, vol. 40, no. 3, pp. 1093–1099, Jul. 2004.

[24] R. L. Streit and T. E. Luginbuhl, "Maximum likelihood method for probabilistic multihypothesis tracking," *Proc. SPIE*, vol. 2235, pp. 394–405, 1994.

[25] L. Herrmann, Á. F. Garcıá-Fernández, and E. F. Brekke, "Histogram-probabilistic multi-hypothesis tracking with integrated target existence," 2025, in *IEEE Trans. Aerosp. Electron. Syst.*.

[26] L. Lindenmaier, S. Aradi, T. Bécsi, and B. Fekete, "Comparison of track management strategies in automotive track-to-track fusion algorithms," in *Proc. IEEE 23 rd World Symp. Appl. Mach. Intell. Inform.*, 2025, pp. 00377–00384.

[27] E. F. Wilthil, E. Brekke, and O. B. Asplin, "Track initiation for maritime radar tracking with and without prior information," in *Proc. 21st Int. Conf. Inf. Fusion*, 2018, pp. 1–8.

[28] M. Sedehi, P. Lombardo, and A. Farina, "A modified m/n logic for track initiation of low observable targets using amplitude information," in *Proc. Int. Radar Symp.*, 2006, pp. 1–4.

[29] M. Wieneke and W. Koch, "On sequential track extraction within the PMHT framework," *EURASIP J. Adv. Signal Process.*, vol. 2008, no. 1, 2007, Art. no. 276914.

[30] M. Maehlisch, W. Ritter, and K. Dietmayer, "De-cluttering with integrated probabilistic data association for multisensor multitarget acc vehicle tracking," in *Proc. IEEE Intell. Veh. Symp.*, 2007, pp. 178–183.

[31] R. O. Chavez-Garcia, J. Burlet, T.-D. Vu, and O. Aycard, "Frontal object perception using radar and mono-vision," in *Proc. IEEE Intell. Veh. Symp.*, 2012, pp. 159–164.

[32] The MathWorks Inc., "Sensor fusion and tracking toolbox: 24.1 (R2024a)," Natick, MA, USA, 2026. [Online]. Available: https://www.mathworks.com

[33] D. Mušicki, T. L. Song, H. H. Lee, X. Chen, and T. Kirubarajan, "Track-to-track fusion with target existence," *IET Radar, Sonar Navigation*, vol. 9, no. 3, pp. 241–248, 2015.

[34] E. H. Lee and T. L. Song, "Multi-sensor track-to-track fusion with target existence in cluttered environments," *IET Radar, Sonar Navigation*, vol. 11, no. 7, pp. 1108–1115, 2017.

[35] M. Aeberhard, S. Paul, N. Kaempchen, and T. Bertram, "Object existence probability fusion using Dempster-Shafer theory in a high-level sensor data fusion architecture," in *Proc. IEEE Intell. Veh. Symp.*, 2011, pp. 770–775.

[36] M. Aeberhard, *Object-Level Fusion for Surround Environment Perception in Automated Driving Applications, 5.2.2 Modeling with Dempster-Shafer Evidence Theory*. Düsseldorf, Germany: VDI Verlag, 2017, pp. 105–110.

[37] A. P. Dempster, "Upper and lower probabilities induced by a multivalued mapping," in *Classic Works of the Dempster-Shafer Theory of Belief Functions*. Berlin, Germany: Springer, 2008, pp. 57–72.

[38] L. Lindenmaier, B. Czibere, S. Aradi, and T. Bécsi, "A robust and runtime-efficient track-to-track fusion for automotive perception systems," *IEEE Sensors J.*, vol. 25, no. 8, pp. 14022–14035, Aug. 2025.

[39] L. Lindenmaier, S. Aradi, T. Bécsi, O. Törő, and P. Gáspár, "GM-PHD filter based sensor data fusion for automotive frontal perception system," *IEEE Trans. Veh. Technol.*, vol. 71, no. 7, pp. 7215–7229, Jul. 2022.

[40] C. Otto, *Fusion of Data From Heterogeneous Sensors With Distributed Fields of View and Situation Evaluation for Advanced Driver Assistance Systems*, vol. 8. Karlsruhe, Germany: KIT Sci. Publishing, 2014.

[41] M. Munz, M. Mählisch, J. Dickmann, and K. Dietmayer, "Probabilistic modeling of sensor properties in generic fusion systems for modern driver assistance systems," in *Proc. IEEE Intell. Veh. Symp.*, 2010, pp. 760–765.

[42] M. Aeberhard, *Object-Level Fusion for Surround Environment Perception in Automated Driving Applications, 5.1.4 Modeling the Parameters*. Düsseldorf, Germany: VDI Verlag, 2017, pp. 98–104.

[43] O. Törmath2, T. PLX Bécsi, and P. Gáspár, "PHD filter for object tracking in road traffic applications considering varying detectability," *Sensors*, vol. 21, no. 2, 2021, Art. no. 472.

[44] S. Matzka and R. Altendorfer, "A comparison of track-to-track fusion algorithms for automotive sensor fusion," in *Proc. IEEE Int. Conf. Multisensor Fusion Integration Intell. Syst.*, 2008, pp. 189–194.

[45] A. Jøsang and S. Pope, "Dempster's rule as seen by little colored balls," *Comput. Intell.*, vol. 28, no. 4, pp. 453–474, 2012.

[46] L. Lindenmaier, S. Aradi, T. Bécsi, O. Törő, and P. Gáspár, "Object-level data-driven sensor simulation for automotive environment perception," *IEEE Trans. Intell. Veh.*, vol. 8, no. 10, pp. 4341–4356, Oct. 2023.

[47] L. Lindenmaier, S. Aradi, T. Bécsi, and P. Gáspár, "Semi-automatic BEV ground truth generation for automotive perception systems," *IEEE Trans. Intell. Veh.*, vol. 10, no. 2, pp. 1441–1454, Feb. 2025.

JENŐ BÓKA received the B.Sc. degree in electrical engineering from Óbuda University, Budapest, Hungary, in 2015, and the M.Sc. degree in electrical and electronics engineering from the Budapest University of Technology and Economics, Budapest, in 2018. From 2018 to 2021, he was with Knorr-Bremse, focusing on automotive environment perception, high-performance sensor data processing, and real-time embedded implementations for safety-critical platforms. Since 2021, he has been with VIE Technology Europe as a Technical Specialist Engineer, developing ADAS functions from concept to series production. He is the author and co-author of multiple patents in autonomous vehicle systems. His research interests include multi-sensor data fusion, Bayesian state estimation, vehicle control, and high-performance algorithm development.

LÁSZLÓ LINDENMAIER received the M.Sc. and Ph.D. degrees from the Budapest University of Technology and Economics, Budapest, Hungary, in 2020 and 2026, respectively. From 2017 to 2020, he was a Development Engineer with Knorr-Bremse, focusing on automotive environment perception and sensor data fusion. Since 2021, he has been an Assistant Research Fellow with the Department of Control for Transportation and Vehicle Systems. Since 2025, he has also been with VIE Technology Europe, Budapest, where he is currently a Technical Specialist Engineer. His research interests include vehicle control, automotive environment perception, object detection, Bayesian state estimation, multi-object tracking, and multi-sensor data fusion.

SZILÁRD ARADI (Senior Member, IEEE) received the M.Sc. and Ph.D. degrees from the Budapest University of Technology and Economics, Budapest, Hungary, in 2005 and 2015, respectively. He has been an Associate Professor with the Department of Control for Transportation and Vehicle Systems, Budapest University of Technology and Economics since 2021 and Senior Lecturer since 2026. His research interests include embedded systems, communication networks, vehicle mechatronics, reinforcement learning, railway information systems, vehicle on-board networks, and vehicle control.

TAMÁS BÉCSI (Senior Member, IEEE) received the M.Sc. and Ph.D. degrees from the Budapest University of Technology and Economics, Budapest, Hungary, in 2002 and 2008, respectively. Since 2005, he has been with the Department of Control for Transportation and Vehicle Systems, Budapest University of Technology and Economics, initially as an Assistant Lecturer and subsequently as an Associate Professor, in 2014. In 2025, he was the Head of Department. His research interests include linear systems, traffic modeling, and simulation, and machine learning, with significant contributions to both academic research and industrial projects in railway information systems and vehicle control.